Interface-Induced Topological Insulator Transition in GaAs/Ge/GaAs Quantum Wells

Dong Zhang,[1] Wenkai Lou,[1] Maosheng Miao,[2] Shou-cheng Zhang,[3] and Kai Chang[1,4,*]

[1]*SKLSM, Institute of Semiconductors, Chinese Academy of Sciences, P.O. Box 912, Beijing 100083, China*

[2]*Materials Research Laboratory and Materials Department, University of California, Santa Barbara, California 93106-5050, USA*

[3]*Department of Physics, Stanford University, Stanford, California 94305, USA*

[4]*Beijing Computational Science Research Center, Beijing 100084, China*

(Received 3 July 2013; published 11 October 2013)

We demonstrate theoretically that interface engineering can drive germanium, one of the most commonly used semiconductors, into a topological insulating phase. Utilizing giant electric fields generated by charge accumulation at GaAs/Ge/GaAs opposite semiconductor interfaces and band folding, the new design can reduce the sizable gap in Ge and induce large spin-orbit interaction, which leads to a topological insulator transition. Our work provides a new method to realize topological insulators in commonly used semiconductors and suggests a promising approach to integrate it in well-developed semiconductor electronic devices.

DOI: 10.1103/PhysRevLett.111.156402 PACS numbers: 71.70.Ej, 72.25.Mk, 75.76.+j

Time-reversal invariant topological insulators (TIs) have aroused intense interest in the past years, with tantalizing properties such as insulating bulk, robust metallic edge or surface modes, and exotic topological excitations, and potential applications ranging from spintronics to quantum computation [1–15]. Despite these successful progresses, the topological insulator materials are still limited in the narrow gap materials containing heavy atoms, e.g., HgTe [4,5], Bi_2X_3 ($X = Se, Te, \ldots$) [8–11], transition metal oxide heterostructure [16], and Heusler compounds [12,17]. These materials are often very different from conventional semiconductor materials in structures and properties and are hard to integrate in current electronics devices that are based on well-developed semiconductor fabrication technologies.

Although there are theoretical predictions about realizing TI states in graphene [3,18,19], the main obstacle is the weak intrinsic spin-orbit interaction (SOI) of carbon atoms. Here, instead of searching new TI materials with exotic structures and chemical elements, we take a totally different route: driving the commonly used semiconductors into TI states by using the intrinsic electric field and the strains. The difficulty of this approach lies in the fact that most of the commonly used semiconductors, such as Si, Ge, GaAs, and many others, usually possess sizable band gaps and do not have strong enough SOI. Furthermore, group IV elements such as Si and Ge have indirect band gap, posing extra difficulty in realizing TI. Inspired by recent theoretical works that the normal insulator [20] can be driven into a TI by an external electric field, our approach is to impose a huge electric field by deliberately designed heterostructures. Recently, an interesting way of realizing a topological insulating phase in a p-type GaAs quantum well (QW) by two-dimensional superimposed potentials with hexagonal symmetry was proposed [21]. Different from that work, our approach relies completely on the material engineering at the atomic level.

Since commonly used semiconductors, e.g., Si, Ge, GaAs, posses a sizable band gap ranging from 0.8 to 1.4 eV, a huge electric field is required to close the band gap and even invert the conduction and valence bands. Such a huge electric field cannot be generated utilizing the gate technique. However, recent technical advances in the atomic-scale synthesis makes it possible to fabricate high quality semiconductor and oxide heterostrutures. It provides us with abundant opportunities to create novel quantum states and emergent phenomena at the interfaces by reconstructing charge, spin, and orbital states. Very recently, a new way to explore a topological insulating phase in semiconductors was proposed utilizing a strong piezoelectric effect at the interface between GaN and InN [22]. The strain between these material results in a huge polarization and electric field across the interfaces. This huge electric field not only can invert the conduction and valence bands, but also generates strong Rashba SOI, eventually driving the system into a topological insulating phase. Strong strain ($\sim 10\%$) in this system may cause two opposite effects, since it drives the system into a topological insulating phase, but the release of the strain can also induce defect, vacancy, and dislocation in the samples, the density of these defects increases rapidly as the thickness of InN layers increases, making the sample growth and fabrication very challenging. To overcome this obstacle, it would greatly advance the field if one could realize the topological insulator in lattice-matched common semiconductors.

Ge and GaAs are both important materials for microelectronic and optoelectronic device applications. Very recently, Ge/GaAs heterostructures realized by epitaxy methods paved the way to heterostructure based devices utilizing the band offsets, quantum size effects, and band structure modifications by electric fields. Ge/GaAs

quantum structures promise the dramatic mobility increase needed for power saving electronics [23–26]. Ge/GaAs interfaces with exceedingly small lattice mismatch posses many advantages over the strained interface. Ge layers grown on GaAs substrate were studied because of their widespread applications in solar cells [27], metal-oxide-semiconductor field-effect transistors [28]. millimeter-wave mixer diodes [29], temperature sensors [30], and photodetectors [31].

Considering a GaAs/Ge/GaAs QW grown along the polar direction [111] (see Fig. 1), a large electric field can be induced in the sandwiched Ge layer. In a GaAs/Ge/GaAs QW, one interface consists of As-Ge bonds and the other consists of Ga-Ge bonds. Because each As contains five electrons whereas Ga contains only three, charge will transfer from the As-Ge side to the Ga-Ge side and a large electric field will be created and imposed on the Ge layer. The electric field will shift the electron and the hole states to the left and right sides of the QW and reduce their energy difference (band gap), and may eventually invert their order. In addition, the electric field also induces a considerably large Rashba SOI.

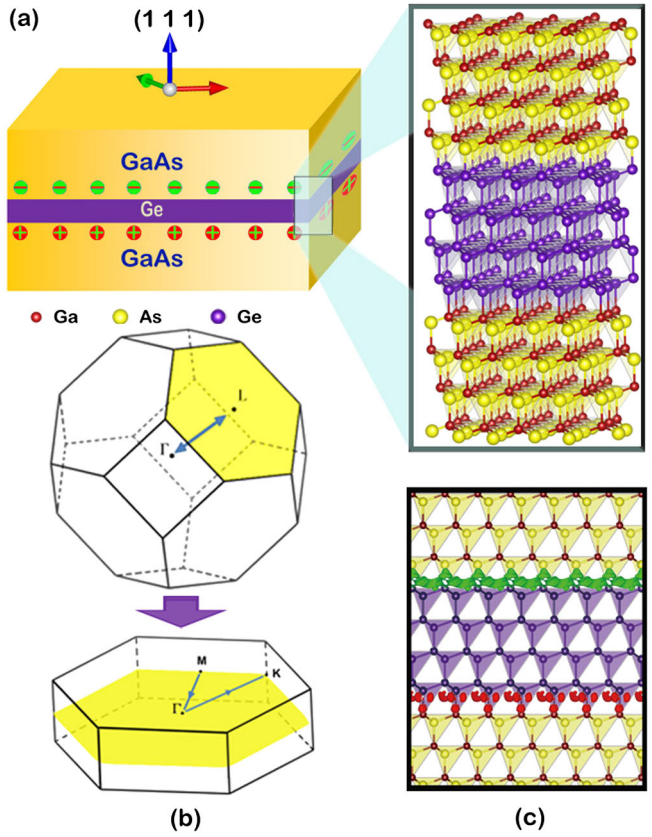

FIG. 1 (color online). (a) Schematic of the structure of an ultrathin Ge layer sandwiched by thick GaAs layers (the upper left-hand panel). The upper right-hand panel amplifies the atomic configuration of the GaAs/Ge/GaAs quantum well containing four bilayer Ge. Notice that the Ga and As atoms locate at the opposite interfaces which leads to a charge accumulation schematically shown in the left-hand panel. (b) The BZ of bulk Ge and the folded BZ of GaAs/Ge/GaAs QW along the [111] crystallographic direction. (c) The charge accumulation at two opposite interfaces obtained from the first-principles calculation. The red and green isosurfaces describe the positive and negative charge accumulations at opposite interfaces.

In order to demonstrate the TI transition in GaAs/Ge/GaAs, we employ two complementary approaches: the first-principles methods based on density functional theory (DFT) and the multiband $\mathbf{k}\cdot\mathbf{p}$ theory. In the first approach, the GaAs/Ge/GaAs structure is modeled by a series of supercells consisting of 15 atomic bilayers in which the thickness of the Ge layer varies from one bilayer to six bilayers (periodicity requires that the total number of atomic layers be even). Because of the key importance of the band gaps, we use a hybrid functional in Heyd-Scuseria-Ernzerhof (HSE) scheme, an approach that has been proved to yield band gaps in good comparison with experimental values for the majority of semiconductor materials [32,33], as implemented in the VASP program [34]. Using a standard mixing parameter of 0.25, we found the band gaps of GaAs and Ge to be 1.08 and 0.73 eV (Ref. [35]). The lattice parameters $a = b = c$ are found to be 5.655 Å for GaAs and 5.657 Å for Ge. On the other hand, SOI is not included in our DFT calculations because of the exceedingly large computing demand while combining HSE and SOI. Instead, we adopt a 30-band $\mathbf{k}\cdot\mathbf{p}$ Hamiltonian with SOI and apply it to the GaAs/Ge/GaAs QWs. The 30-band $\mathbf{k}\cdot\mathbf{p}$ model was used to calculate the band structure of commonly used semiconductors in the whole Brillouin zone [36–38].

The proposed GaAs/Ge/GaAs structure is shown schematically in Fig. 1(a), together with the inset showing the atomic structure of the GaAs/Ge interfaces along the (111) growth direction. As is well known, Ge is an indirect semiconductor with the valence band maximum at the Γ point and the conduction band minimum at the L point. While growing a heterojuction along the (111) direction, the symmetries are broken and the bands are folded along the Γ-L direction [see Fig. 1(b)]. As a result, the conduction band minimum at the L points in bulk Ge is folded to the Γ point and the Ge thin layers growing in the (111) direction possess a direct gap at Γ. The band folding is nontrivial, as we will show below in both the DFT calculation and the $\mathbf{k}\cdot\mathbf{p}$ model, and the breaking of the cubic symmetry also leads to a strong coupling between the electron and the hole states, which is essential for the TI transition.

Figure 2(a) presents the HSE band structures of GaAs/Ge/GaAs QW with two and four bilayers of Ge. The two-Ge-bilayer QW has a gap of 0.8 eV that is comparable to the direct gap of Ge at the Γ point. At four Ge bilayers, the gap decreases to 0.3 eV. The large remaining band gap is the result of a strong quantum confinement effect, which will decrease with the increasing Ge layer thickness. In both of these cases, the band structures still display normal order in the sense that the heavy hole (HH)

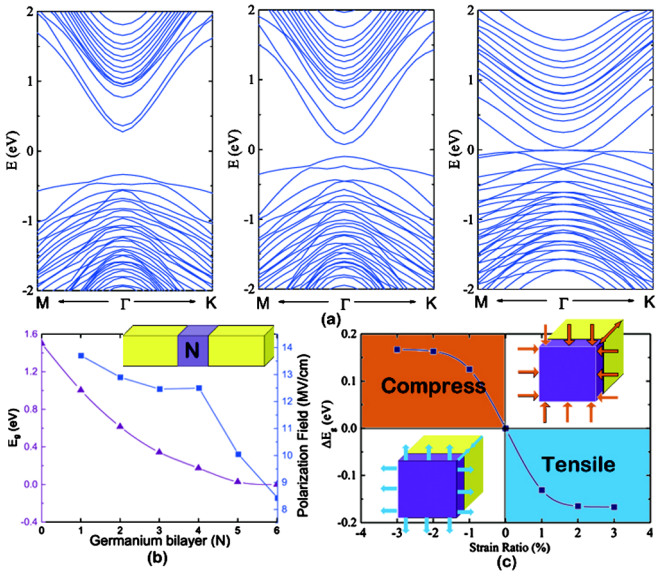

FIG. 2 (color online). (a) Band structures of GaAs/Ge/GaAs sandwiched structures with different Ge portions obtained from the first-principles HSE calculations. From left to right, two Ge bilayers, four Ge bilayers, and four Ge bilayers with 3% in-plane tensile strain. (b) The band gap (purple line with diamonds) and the inner polarization field strength (blue line with squares) as functions of the number of Ge bilayers. (c) The variation of band gap $\Delta E_g = E_g^{\text{strain}} - E_g$ as a function of in-plane strain.

and light hole (LH) states are degenerate at the Γ point (Γ_5) and are lower in energy than the electron state (E) (Γ_1). As a matter of fact, our HSE calculations show that the charge field itself cannot drive the system into inverted bands. As shown in Fig. 2(c), the band gap keeps decreasing but remains positive with up to six bilayers of Ge.

The driving force of the decreasing band gap is the strong electric field imposed by the charges located at the two interfaces in GaAs/Ge/GaAs QW [see Fig. 1(c)]. In principle, the strength of the electric field should not change with increasing thickness of the Ge layer. However, because of the finite size of our supercell, the actual model in the HSE calculations are a GaAs/Ge superlattice, in which the GaAs region is much thicker than the Ge region. For that reason, the electric field goes down slightly with increasing Ge thickness. This feature is well captured by the HSE calculations as shown in Fig. 2(c). While the QW contains more than four Ge bilayers, the HSE calculations show that the electric field goes down dramatically. It decreases from 12.5 MV/cm for four Ge bilayers to 8.5 MV/cm for six Ge bilayers. The decreasing electric field is a result of charge transfer from the Ga-Ge interface to the As-Ge interface, which weakens the driving force toward band inversion.

While the bands of the GaAs/Ge/GaAs QW remain in normal order with increasing Ge thickness, we found that a slight tensile strain is enough to drive the system into inverted bands. As shown in the upper right-hand panel of Fig. 2(a), the system exhibits an inverted band structure, in which Γ_5 states are 0.1 eV higher than the Γ_1 state for four Ge bilayers with 1% tensile strain, and 0.2 eV for 2% strain. The actual band inversion can happen under a much smaller strain. This slight tensile strain can be realized by doping In atoms into GaAs host material, bending the sample, or growing the heterostructures on a substrate with larger lattices. In Fig. 2(b), the states around the Γ point are still denoted as E, HH, and LH according to its energy order, which is different from the notation used in previous works [4]. Such an inverted band structure is a signature of the transition to a TI state. Similar to bulk Ge, the effect of the strains on the band gaps of GaAs/Ge/GaAs QW are quite strong. As shown in Fig. 2(c), the band gap can change for about 0.2 eV with 2% compressive and tensile strains, providing us with an effective way to control the TI transition.

Although the HSE band structure calculations show that the combination of the strong electric field and a modest strain can invert the bands of GaAs/Ge/GaAs QW at the Γ point, it is not sufficient to prove the TI transition. In order to show the TI transition, both band inversion and the SOI should present. The calculation of band structure at the hybrid functional level with SOI for a QW system is extremely demanding on computing resources. We therefore take another approach by constructing a multiband $\mathbf{k}\cdot\mathbf{p}$ model Hamiltonian. The parameters of the model are carefully calibrated with HSE calculations. Comparing with a HgTe system, there are more valence bands involved in interacting with the electron state at the Γ point. We find that the inclusion of 30 bands in total is sufficient to describe complicated interband coupling at the Γ point of the Brillouin zone of GaAs/Ge/GaAs QWs. The most important states near the band gap are the spin-up and spin-down electron states ($|E,\uparrow\rangle$ and $|E,\downarrow\rangle$) and the spin-up and spin-down heavy hole ($|\mathrm{HH},\uparrow\rangle$ and $|\mathrm{HH},\downarrow\rangle$) states. We would like to emphasize that the electron and heavy hole subbands ($|E,\uparrow\downarrow\rangle$ and $|\mathrm{HH},\uparrow\downarrow\rangle$) denote only the dominant components of the lowest conduction and highest valence subbands and are mixed with electron and heavy and light hole states due to the interband coupling in the $\mathbf{k}\cdot\mathbf{p}$ theory.

By applying the $\mathbf{k}\cdot\mathbf{p}$ theory, we first confirm the band inversion in the GaAs/Ge/GaAs QW system. The numerical simulation shows that the inversion happens when the thickness of the Ge layer is larger than 18 Å and the QW is subject to about 0.5% tensile strain. This corresponds to about four Ge bilayers and is in excellent agreement with the HSE results. The inverted bands are shown in Fig. 3(a); the electron Γ_1 state is lower in energy than the valence Γ_5 state. Clearly, it is the result of the fact that the highest valence subbands $|\mathrm{HH},\uparrow\downarrow\rangle$ are heavily involved in the coupling with electronic subbands $|E,\uparrow\downarrow\rangle$ near the Γ point.

Spin-orbit interaction is essential in the transition to a TI state. The intrinsic SOIs in both Ge and GaAs are not strong

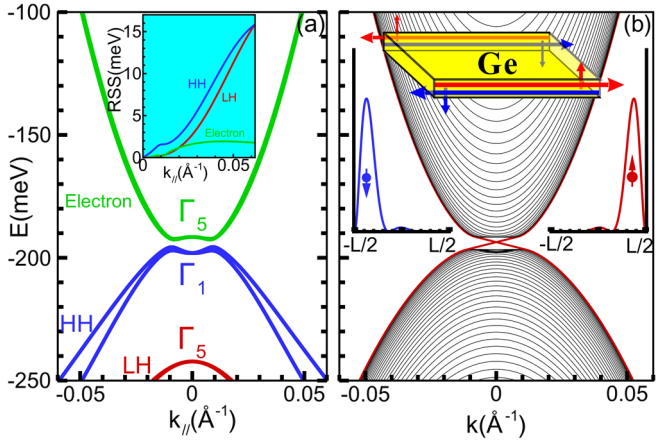

FIG. 3 (color online). (a) Band structures of a GaAs/Ge/GaAs QW structure with 18 Å Ge layer thickness obtained from the 30-band $\mathbf{k}\cdot\mathbf{p}$ model. The inset shows the Rashba spin splitting (RSS) of electron, heavy hole (HH), and light hole (LH). (b) Band structure of the quantum wire obtained by solving the effective four-band model. The gapless edge states are shown by the red line. The central inset shows the schematic of the quantum wire and the helical edge states. The right (red) and left peaks (blue) describe the density distribution of the spin-up and spin-down edge states at $k_{\|} = -0.01$ Å^{-1}, respectively.

enough to create TI states. We found that the large interface electric field induces a considerably large Rashba SOI splitting from the 30-band $\mathbf{k}\cdot\mathbf{p}$ theory for electron and hole states [$\sim$ 2–15 meV, see the inset of Fig. 3(a)], respectively. The magnitude is comparable with that in HgTe QWs [20]. This large Rashba SOI in GaAs/Ge/GaAs QW is a natural result of the strong electric field and can be derived from the multiband $\mathbf{k}\cdot\mathbf{p}$ theory. No fitting parameters are required except the strength of the electric field, which is adopted from the HSE DFT calculation [see Fig. 2(b)]. The strong Rashba SOI in QWs provides a controllable approach to create TI states in GaAs/Ge/GaAs QWs. The strengths of the Rashba SOI in the GaAs/Ge/GaAs QWs are comparable to the Rashba spin splitting induced by an external electric field in InAs and HgTe quantum wells [20]. A Rashba SOI of this magnitude usually occurs only in systems containing heavier atoms. The unusually large Rashba SOI in GaAs/Ge/GaAs QWs is due to the strength of the polarization field, which easily exceeds 10 times the strength of an applied electric field resulting from the state-of-the-art gate technique.

Next, we will demonstrate the topological insulator transition in this GaAs/Ge/GaAs QW system. The light hole subbands with the dominant components $|\mathrm{LH}, \uparrow\downarrow\rangle$ are about 50 meV below the electron and heavy hole subbands ($|E, \uparrow\downarrow\rangle$ and $|\mathrm{HH}, \uparrow\downarrow\rangle$) (see Figs. S2 and S3 in the Supplemental Material [39]). Since we are only interested in the edge states inside the bulk gap ($\sim$ 10 meV), the light hole subbands $|\mathrm{LH}, \uparrow\downarrow\rangle$ are not necessary to be explicitly included when we reduce the multiband $\mathbf{k}\cdot\mathbf{p}$ model to the effective 2D $\mathbf{k}\cdot\mathbf{p}$ model. We down fold the 30-band model Hamiltonian to an effective 2D four-band Hamiltonian expressed in the above four bases ($|E, \uparrow\downarrow\rangle$ and $|\mathrm{HH}, \uparrow\downarrow\rangle$). The exact form and the derivation process of the four-band effective 2D Hamiltonian can be found in the Supplemental Material [39]. The contributions from the lowest and highest ten subbands are included in this four-band reduced Hamiltonian via the Löwdin perturbation theory [40]. The explicit expression of the four-band effective 2D Hamiltonian in the basis $|E_1, \uparrow\rangle$, $|\mathrm{HH}_1, \uparrow\rangle$ is

$$H^{\mathrm{eff}}_{4\times4} = \begin{bmatrix} E_0 + E_1 k_{\|}^2 & A_1 k_+ & 0 & 0 \\ A_1^* k_- & H_0 + H_1 k_{\|}^2 & 0 & 0 \\ 0 & 0 & E_0 + E_1 k_{\|}^2 & -A_1 k_- \\ 0 & 0 & -A_1^* k_+ & H_0 + H_1 k_{\|}^2 \end{bmatrix}, \quad (1)$$

where $k_{\|}$ denotes the in-plane momentum, $k_+ = k_x \pm i k_y$, and the relevant parameters are $E_0 = -0.198\,08$ eV, $E_1 = 0.438\,10$ eV $\cdot$ Å^2, $H_0 = -0.191\,53$ eV, $H_1 = -0.208\,10$ eV $\cdot$ Å^2, $A_1 = 0.028\,510$ eV $\cdot$ Å.

From the above four-band effective Hamiltonian, we can start to study the topological insulator transition in such 2D QWs. The essential feature of a 2D TI is the existence of the helical edge states near the boundary of the 2D TI sample. We consider a quantum wire structure with a width of 1000 Å. The thickness along the (111) growth direction consists of a Ge layer of 18 Å, sandwiched by two 200 Å GaAs layers. Figure 3(b) shows the band structure of the above quantum wire together with the density distribution of a Kramers pair of edge states. As shown in the figure, the new energy branches appear and sweep across the bulk gap; these states are highly localized near the edge of the quantum wire. The spin-up and spin-down edge states with the same in-plane momentum $k = 0.01$ Å^{-1} along the quantum wire localize at the opposite edges, in contrast to the chiral edge states in the integer quantum Hall effect, where the spin-up and spin-down electron with the same in-plane momentum localizes at the same edge. The presence of these helical edge states clearly demonstrates the TI transition in this two-dimensional GaAs/Ge/GaAs QW system.

The experimental detection of the aforementioned edge states in GaAs/Ge/GaAs Hall bar can be performed in the standard four terminal measurements. The edge states can be observed at the mini gap opened between the $E1$ and the HH1 bands. According to our calculations using the $\mathbf{k}\cdot\mathbf{p}$ model, this mini gap can be as large as 15 meV, which is already larger than the similar mini gap in the InAs/GaSb QW system, another 2D TI in which the edge states have recently been observed [7]. The presence of the TI state in Ge ultrathin layers can largely advance the application of this new quantum state in existing electronics and opto-electronics devices. It shows a considerable advantage over other TI systems including graphene [3], HgTe QW [4,5],

the Bi chalcogenides [9], and the Heusler compounds [12,17]. GaAs/Ge/GaAs sandwiched structures are ready to be integrated with conventional semiconductors which are already extensively used in electronic devices [23–31]. The imposed electric field can be controlled by applying an extra electric field or by inducing holes or electrons into the QW region via a gate voltage, providing us a direct way of manipulating the TI transition in the device. The transition point can also be adjusted by well-developed semiconductor techniques such as alloying and doping.

This work was supported by the NSFC Grants No. 10934007 and No. 2011CB922204 from the MOST of China. M. M. is supported by the MRSEC Program (NSF-DMR1121053) and the ConvEne-IGERT Program (NSF-DGE 0801627). S.-c. Z. is supported by the DARPA Program No. N66001-12-1-4034. K. C. would like to thank Professor Bangfen Zhu, Professor Qikun Xue, Professor Zhong Fang, and Professor Xi Dai for their valuable discussions. D. Zhang and W. Lou contributed equally to this work.

*Corresponding author.
kchang@semi.ac.cn

[1] M. Z. Hasan and C. L. Kane, Rev. Mod. Phys. **82**, 3045 (2010).
[2] X. L. Qi and S. C. Zhang, Rev. Mod. Phys. **83**, 1057 (2011).
[3] C. L. Kane and E. J. Mele, Phys. Rev. Lett. **95**, 146802 (2005).
[4] B. A. Bernevig, T. L. Hughes, and S. C. Zhang, Science **314**, 1757 (2006).
[5] M. Konig, S. Wiedmann, C. Brune, A. Roth, H. Buhmann, L. W. Molenkamp, X.-L. Qi, and S.-C. Zhang, Science **318**, 766 (2007).
[6] C. X. Liu, T. L. Hughes, X. L. Qi, K. Wang, and S. C. Zhang, Phys. Rev. Lett. **100**, 236601 (2008).
[7] I. Knez, R.-R. Du, and G. Sullivan, Phys. Rev. Lett. **107**, 136603 (2011).
[8] L. Fu, C. L. Kane, and E. J. Mele, Phys. Rev. Lett. **98**, 106803 (2007).
[9] D. Hsieh, D. Qian, L. Wray, Y. Xia, Y. S. Hor, R. J. Cava, and M. Z. Hasan, Nature (London) **452**, 970 (2008).
[10] Y. L. Chen *et al.*, Science **325**, 178 (2009).
[11] Y. Xia *et al.*, Nat. Phys. **5**, 398 (2009).
[12] S. Chadov, X. Qi, J. Kübler, G. H. Fecher, C. Felser, and S. C. Zhang, Nat. Mater. **9**, 541 (2010).
[13] H. Lin, L. A. Wray, Y. Xia, S. Xu, S. Jia, R. J. Cava, A. Bansil, and M. Z. Hasan, Nat. Mater. **9**, 546 (2010).
[14] M. Franz, Nat. Mater. **9**, 536 (2010).
[15] K. Yang, W. Setyawan, S. Wang, M. B. Nardelli, and S. Curtarolo, Nat. Mater. **11**, 614 (2012).
[16] D. Xiao, W. G. Zhu, Y. Ran, N. Nagaosa, and S. Okamoto, Nat. Commun. **2**, 596 (2011).
[17] D. Xiao, Y. Yao, W. Feng, J. Wen, W. Zhu, X. Q. Chen, G. M. Stocks, and Z. Zhang, Phys. Rev. Lett. **105**, 096404 (2010).
[18] A. H. Castro Neto, F. Guinea, N. M. R. Peres, K. S. Novoselov, and A. K. Geim, Rev. Mod. Phys. **81**, 109 (2009).
[19] Z. Qiao, W. K. Tse, H. Jiang, Y. Yao, and Qian Niu, Phys. Rev. Lett. **107**, 256801 (2011).
[20] W. Yang, K. Chang, and S. C. Zhang, Phys. Rev. Lett. **100**, 056602 (2008); J. Li and K. Chang, Appl. Phys. Lett. **95**, 222110 (2009).
[21] O. P. Sushkov and A. H. Castro Neto, Phys. Rev. Lett. **110**, 186601 (2013).
[22] M. S. Miao, Q. Yan, C. G. Van de Walle, W. K. Lou, L. L. Li, and K. Chang, Phys. Rev. Lett. **109**, 186803 (2012).
[23] R. Pillarisetty, Nature (London) **479**, 324 (2011).
[24] V. F. Mitin, V. K. Lazarov, P. M. Lytvyn, P. J. Hasnip, V. V. Kholevchuk, L. A. Matveeva, E. Yu. Kolyadina, I. E. Kotenko, V. V. Mitin, and E. F. Venger, Phys. Rev. B **84**, 125316 (2011).
[25] M. K. Hudait, Y. Zhu, N. Jain, S. Vijayaraghavan, A. Saha, T. Merritt, and G. A. Khodaparast, J. Vac. Sci. Technol. B **30**, 051205 (2012).
[26] Y. Huo, H. Lin, R. Chen, M. Makarova, Y. Rong, M. Li, T. I. Kamins, J. Vuckovic, and J. S. Harris, Appl. Phys. Lett. **98**, 011111 (2011).
[27] S. J. Wojtczuk, S. P. Tobin, C. J. Keavney, C. Bajgar, M. M. Sanfacon, L. M. Geoffroy, T. M. Dixon, S. M. Vernon, J. D. Scofield, and D. S. Ruby, IEEE Trans. Electron Devices **37**, 455 (1990).
[28] G.-L. Luo *et al.*, J. Electrochem. Soc. **157**, H27 (2010).
[29] A. Christou, W. T. Anderson, Jr., J. E. Davey, M. L. Bark, and Y. Anand, Electron. Lett. **16**, 254 (1980).
[30] V. F. Mitin, V. V. Kholevchuk, and B. P. Kolodych, Cryogenics **51**, 68 (2011).
[31] V. F. Mitin, Yu. A. Tkhorik, and E. F. Venger, Microelectron. J. **28**, 617 (1997).
[32] P. E. Blöchl, Phys. Rev. B **50**, 17 953 (1994).
[33] J. Heyd, G. E. Scuseria, and M. Ernzerhof, J. Chem. Phys. **118**, 8207 (2003).
[34] G. Kresse and J. Furthmuller, Phys. Rev. B **54**, 11 169 (1996).
[35] J. E. Peralta, J. Heyd, G. E. Scuseria, and R. L. Martin, Phys. Rev. B **74**, 073101 (2006).
[36] M. Cardona, N. E. Christensen, and G. Fasol, Phys. Rev. B **38**, 1806 (1988).
[37] S. Richard, F. Aniel, and G. Fishman, Phys. Rev. B **70**, 235204 (2004).
[38] M. El Kurdi, S. Sauvage, G. Fishman, and P. Boucaud, Phys. Rev. B **73**, 195327 (2006).
[39] See Supplemental Material at http://link.aps.org/supplemental/10.1103/PhysRevLett.111.156402 for details of 30-band $\mathbf{k}\cdot\mathbf{p}$ theory.
[40] P. O. Löwdin, J. Chem. Phys. **19**, 1396 (1951).